Laboratory Tests Assessment of a Mechanical Sensor-less MPPT Control Strategy for Tidal Turbines

Mohammad Rafiei, Francesco Salvatore, Carwyn Frost, and Ian Benson

Abstract—**The purpose of this study is to demonstrate through towing tank experiments the effectiveness of a novel mechanical sensor-less Maximum Power Point Tracking (MPPT) control for tidal stream turbines under fluctuations of the onset flow. The MPPT control method, based on the linear relationship between DC outputs of a Permanent Magnet Synchronous Generator (PMSG), was derived theoretically and validated through model tests. The tests were conducted under both steady-state and unsteady inflow conditions, using the 1.5 m diameter horizontal-axis device developed at the Queen's University of Belfast. Results indicate that the proposed MPPT control strategy improves the convergence to the maximum power coefficient under regular wave conditions, thereby validating its efficacy. A comparative analysis with a conventional Tip Speed Ratio (TSR) control method is also presented.**

Index Terms—**Tidal energy, MPPT control strategy, PMSG, Wave-current interaction, Towing tank tests.**

I. Introduction

OCEAN energy will play a crucial role in the renewable energy sector over the next decades. Instream turbines for tidal currents are a rapidly maturing technology to exploit a highly predictable energy source [1]. Despite the promising prospects of tidal energy, substantial challenges persist in terms of optimizing reliability and efficiency. Tidal Stream Turbines (TSTs) face significant hurdles due to transient loads caused by inflow velocity fluctuations, which can lead to fatigue, thus affecting system longevity and lifecycle efficiency [2]. These fluctuations are often attributed to various transient phenomena in the tidal stream, including waves [3] and turbulence [4].

In laboratory tests, fully controllable and repeatable fluctuations of the onset flow velocity can be generated by generating surface waves propagating against the model turbine. A comprehensive characterization of onset flow perturbations induced by surface waves can be obtained under linear wave theory assumptions, as discussed, *e.g.*, in [5].

Several experimental studies [5]–[9] have been conducted in controlled laboratory settings such as flume or towing tanks to gain insight into the impact of wave-current interactions on turbine performance. These studies assess the performance and operational responses of devices through tests on scale models.

In [5], a 0.5 m diameter model of a horizontal axis tidal turbine was tested under regular surface waves. Despite similar mean coefficients of power and thrust were measured in unsteady and steady flow conditions, significant cyclic variations in power and thrust were observed at the frequency of the waves. On the other hand, [6] highlighted the potential of transient interactions between tidal currents and turbine rotation to induce high asymmetric loadings, which could lead to early component failure. This study emphasized the importance of understanding flow regimes for material selection and deformation capability of turbine blades. Knowledge gained from these studies can aid fatigue prediction and component lifespan estimation, providing crucial data for turbine design.

An investigation on extreme wave-current conditions in [7] revealed significant variations in power. Time histories of blade root loading in wave-current conditions highlighted the importance of relationships between wave phase, blade angular position, and the number of blade rotational periods in a wave period for the fatigue life of the blade. Moreover, the authors in [8] carried out the first experimental investigation of a horizontal axis turbine model subjected to combined oblique waves and current. The findings showed that the presence of waves significantly affected the rotor power and thrust, with off-axis waves associated with lower thrust loads than head-on waves.

Recently, a Round Robin Test program [9] demonstrated the influence of the combined wave and current effect on the power capture and performance of a notional model turbine. The performance varied between facilities, with differences up to 25% in terms of average power coefficient depending on the wave and current cases.

This body of research provides valuable insights into the performance and operational responses of tidal stream turbines under various wave-current conditions. Furthermore, the knowledge gained from these experiments, underscores the necessity for comprehensive testing and further reinforces the importance of

This work was partially supported by the H2020 MaRINET-2 project under EU grant 731084'

Mohammad Rafiei is with the Institute of Marine Engineering of the National Research Concil of Italy, Via di Vallerano 139, 00128 Rome, Italy (e-mail: mohammad.rafiei@inm.cnr.it).

Francesco Salvatore is with the Institute of Marine Engineering of the National Research Concil of Italy, Via di Vallerano 139, 00128 Rome, Italy (e-mail: francesco.salvatore@cnr.it).

Carwyn Frost is with the School of Natural and Built Environment, Queen's University, Belfast, Northern Ireland, United Kingdom (e-mail: c.frost@qub.ac.uk).

Ian Benson is with the School of Natural and Built Environment, Queen's University, Belfast, Northern Ireland, United Kingdom (e-mail: ianfwd@tutanota.com).

Digital Object Identifier:
https://doi.org/10.36688/ewtec-2023-434

well-designed control strategies to optimize turbine operation in varying environmental contexts.

Control strategies based on Maximum Power Point Tracking (MPPT) are utilized to maximize the electrical power production of rotary-wing energy generators, as *e.g.*, wind turbines and TSTs. Assuming the optimal Tip Speed Ratio (TSR) corresponding to the maximum power coefficient is known, the turbine operational state is modulated in the attempt to enforce that the optimal TSR is tracked regardless of the variability of the onset flow and turbine loading conditions. An effectively structured control system for turbine operation not only enhances the device efficiency and lowers the cost of energy generation, but also improves its operational life by mitigating the intensity of oscillations of mechanical loads on rotor blades and drive-train components [10]–[12] . A critical point is the utilization of mechanical sensors to observe inflow fluctuations and turbine operating conditions to feed the control algorithm.

This paper aims to introduce an efficient and robust MPPT control approach that does not rely on mechanical sensors, and instead leverages the linear relationship between the generator DC output current and the square of its voltage. The method requires predetermined turbine characteristics to establish the control reference that is effective across the operating conditions. The proposed model, hereafter referred to as Sensor-Less MPPT (SL-MPPT) was derived theoretically through linearization and simplifications of the turbine power conversion system.

An initial characterization of the SL-MPPT was carried out by tests in the tidal field site in Strangford Narrows, North-Ireland [13], by using the 1.5 m diameter horizontal-axis turbine developed at the Queen's University of Belfast (QUB) [14]. In order to achieve a broader understanding of the effect of control strategies on the turbine performance, in the present work a set of laboratory tests were carried out in the wave-towing tank at CNR-INM, in Rome, Italy, using the same turbine and equipment from field site tests. The laboratory-scale environment of the towing tank provides completely controlled and repeatable testing conditions which allow to perform a careful assessment of the proposed MPPT control strategy and a comparative analysis of different control strategies.

In addition to the proposed SL-MPPT control strategy, laboratory tests also considered a conventional TSR control strategy, in which the angular velocity of the turbine rotor is controlled by measuring the onset flow speed to obtain the optimal TSR and ensure maximum power point tracking.

The tests were conducted in two scenarios: calm water (steady state) and unsteady inflow with a regular (sinusoidal or monochromatic) waveform, with amplitude chosen to simulate moderate sea-state conditions at full scale. The power output was measured from the turbine during regular wave conditions and compared to results from steady flow to assess the impact of wave-induced velocity on turbine performance.

In the following sections, the Power Take Off (PTO) system arrangement of the model turbine, the proposed SL-MPPT control strategy and the logic behind it are briefly explained. The test setup, laboratory test facility, and the test matrix are described. Next, main results describing the turbine operation with the proposed control strategy are presented, and the comparison with results obtained using the conventional TSR control is discussed.

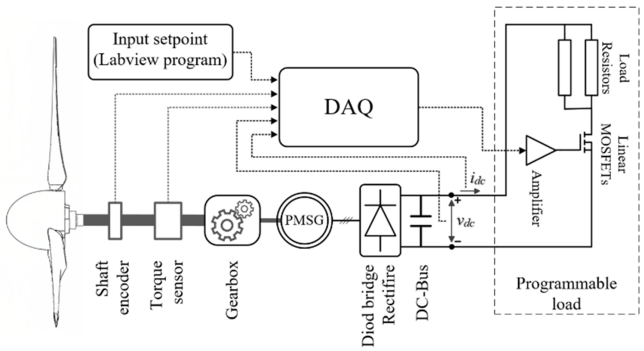

Fig. 1. The power take off layout of the model turbine used in field site and wave–towing tank tests.

II. Methodology

The methodological approach involves the use of a large–scale model turbine, the development of a sensor-less MPPT control strategy for the PTO configuration, and the establishment of specific test scenarios and comparison with a conventional MPPT strategy known as TSR control. These components collectively aim to validate and assess the proposed sensor-less MPPT control strategy for Tidal Stream Turbines (TSTs).

A. Tidal Turbine Testing Device (TTT)

The process of designing and selecting cost-efficient PTO systems is of primary importance for the performance and reliability of tidal turbines. A thorough overview of the latest advancements in tidal turbine generator topologies and PTO layouts was presented in [15]. A direct-drive Permanent Magnet Synchronous Generator (PMSG) with a full-rated frequency converter, combined with fixed-pitch rotor blades, provides an example of a simple and robust PTO configuration.

In the pursuit of tidal turbine research, a large-scale 3-bladed horizontal axis model turbine was built. The device featuring a PTO system tailored to accommodate a 1.5m diameter rotor and a 0.35m diameter nacelle, was developed at the Queen's University Belfast (QUB) [14] and is hereafter referred to as Tidal Turbine Testing (TTT) turbine. Given the rather compact size of the nacelle, the chosen PTO configuration consists of a PMSG coupled with a single-stage gearbox linked to a programmable load via a diode rectifier.

Figure 1 provides a view of the TTT turbine PTO system arrangement. A load-resistor array was implemented to handle the electric power produced by the turbine during operation. To monitor the turbine performance, the generator DC output was measured

using current and volt meters. The demand torque at the DC output terminals was managed using a linear regulator, which was governed by the central Data Acquisition system (DAQ).

The DAQ system, configured on a National Instruments Compact Rio (cRio) and operated with LabVIEW, was upgraded with custom-developed interface electronics and cabling. Moreover, to refine the accuracy of the shaft speed and torque readings, an absolute rotary encoder and a torque meter were implemented. This integration facilitated enhanced precision in the management of the turbine rotor velocity through the Proportional-Integral (PI) loop controller.

B. Sensor-less MPPT control strategy

By using a classical notation, the mechanical power P_m delivered by a turbine can be written in terms of a non dimensional power coefficient C_P as

$$P_m \;=\; \frac{1}{2}\rho A\, C_P V_F^3 \tag{1}$$

where ρ is the water density, R denotes the rotor radius and $A = \pi R^2$ is the rotor swept area, whereas V_F is the nominal onset flow speed.

The turbine operating condition is characterized by the Tip Speed Ratio (TSR) as

$$\lambda \;=\; \frac{\omega_m\, R}{V_F} \tag{2}$$

where $\omega_m = 2\pi n_m$ is the turbine rotational speed, with n_m in rps.

Combining Eqs. (1) and (2), the essence of a MPPT control strategy can be represented by the following equation, which gives a relationship between the maximum mechanical power $P_{m,max}$ that can be harnessed by the turbine rotor, and the corresponding rotational speed $\omega_{m,opt}$

$$\begin{aligned} P_{m,max} &= \frac{1}{2}\rho A\, C_{P,max} \left(\frac{R}{\lambda_{opt}}\right)^3 \omega_{m,opt}^3 \\ &= K_{hy}\, \omega_{m,opt}^3 \end{aligned} \tag{3}$$

where $\lambda_{opt} = \omega_{m,opt} R/V_F$, whereas the quantity K_{hy} is a constant for a given turbine and reference conditions. Recalling that power is directly proportional to torque and angular velocity, Eq. (3) yields

$$Q_{m,opt} \;=\; K_{hy}\, \omega_{m,opt}^2 \tag{4}$$

where $Q_{m,opt}$ represents the optimal mechanical torque of the turbine rotor necessary for extracting the maximum power from the flow.

The Optimum Relation-Based (ORB) control strategy employs pre-set relationships, such as Eq. (4), to track the maximum power point and establish the control reference. This approach has been implemented in the turbines of leading marine renewable energy companies such as ORPC [16] and HydroQuest [17]. However, it's crucial to note that the implementation of this strategy requires the use of mechanical sensors, which could potentially increase the overall cost of the system and affect its reliability.

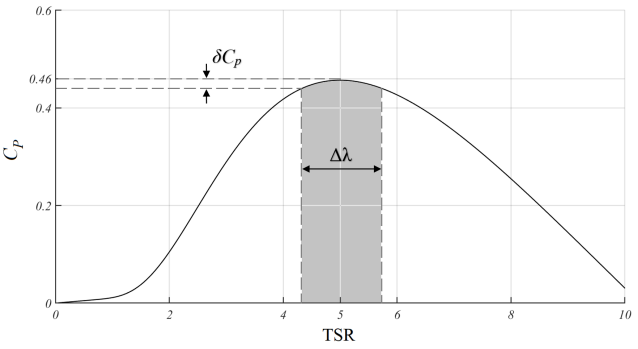

Fig. 2. Notional TST power coefficient curve and TSR-MPPT control region.

Given that electrical torque and DC-bus current I_{dc}, as well as share a proportional relationship, under certain assumptions and simplifications, Eq. (4) can be extended to establish a linear correlation between the generator current and the square of the output voltage. It should be noted that lack of precision of the MPPT control algorithm in pinpointing the optimal operating conditions would cause only a minimal influence on the extracted power. This is visually demonstrated in Fig. 2, where a notional tidal turbine power coefficient curve is charted.

Minor fluctuations in the C_P curve near the maximum power point, coupled with the significant deviation range of turbine rotational speed for a certain inflow velocity, leads to a slight reduction in power. Taking the TTT turbine as example, available towing tank performance data [18] show that a deviation of over 10% around the optimal TSR causes less than a 5% decrease in power. This observation enables us to make simplifications and assumptions in the process of power transmission and conversion from the turbine rotor to the DC side, establishing a linear relationship between the DC-bus current and voltage squared.

The phase back electromotive force E_{mf} of a PMSG with a constant flux Ψ exhibits a linear proportionality to the rotational speed of the generator ω_g

$$E_{mf} \;=\; n_{pp}\, \Psi\, \omega_g \tag{5}$$

where n_{pp} stands for the number of pole pairs. Assuming negligible copper losses, commutating inductance, and commutating angle, the rectifier's output voltage can be simplified as [19]

$$V_{dc} \;=\; \left(\frac{3\sqrt{3}}{\pi}\right) E_{mf} \tag{6}$$

On the other hand, the maximum power output that a diode bridge can provide is represented by

$$V_{dc,opt}\,.\,I_{dc,opt} \;=\; \eta_t\, P_{m,max} \;=\; \eta_t\, K_{hy}\, \omega_{m,opt}^3 \tag{7}$$

where $V_{dc,opt}$ and $I_{dc,opt}$ denote the optimal values of DC-side voltage and current, respectively. Quantity η_t represents the efficiency of power transmission and conversion from the turbine rotor to the DC side, which is assumed to be constant.

The relationship between ω_m and ω_g is defined as

$$\omega_g \;=\; N_{gear}\, \omega_m \tag{8}$$

where N_{gear} denotes the gear ratio for drive-trains equipped with a gearbox. This parameter is set equal to one in the case of direct-drive systems.

By manipulating Eqs. (5)-(8), the following expressions are derived

$$I_{dc,opt} = \eta_t K_{hy} \left[\frac{\pi}{3\sqrt{3} n_{pp} \Psi N_{gear}} \right]^3 V_{dc,opt}^2$$

or simply

$$I_{dc,opt} = K_{dc} V_{dc,opt}^2 \quad (9)$$

where K_{dc} represents the constant slope of the generator output current (I_{dc}) with respect to the square of the generator output voltage (V_{dc}^2), aimed at achieving maximum power. Equation (9) is the basis of the SL-MPPT methodology proposed here, in which only electrical quantities are observed to feed the control strategy.

III. Experimental set-up

This section describes the laboratory infrastructure and the test set-up used to analyse the proposed SL-MPPT control strategy. The primary objective was to examine the SL-MPPT control strategy within a controlled environment that simulates relevant operating conditions at sea. The focus was to understand its response and performance under fluctuating inflow conditions and identify improvements to enhance the turbine power extraction capability. The controlled laboratory environment is crucial as it minimizes the uncertainties associated with field trials, leading to precise and accurate findings. The infrastructure described herein encompasses a towing tank facility and the instrumentation used in the study.

A. Towing tank facility

Laboratory tests were conducted in the wave–towing tank facility at CNR-INM, which is among the largest worldwide for experimental research on marine renewable energy systems. The tank has a length of 220 m, a width of 9 m, and a depth of 3.5 m, resulting in a blockage ratio of 2.8% when the TTT model turbine is deployed. This small blockage ensures that flow confinement effects are negligible, making the results comparable to those obtained in an unbounded environment during sea trials.

The TTT 1.5m diameter, 3-bladed model turbine was equipped with 0.575 m long steel blades by a commercial Schottel Hydro design [20], as shown in Fig. 3. The combination of the TTT model turbine and the towing tank provides an ideal platform for studying tidal stream turbines under controlled conditions.

Wave–towing tank layout and dimensions are illustrated in Fig. 4. The tank is filled with fresh water, and the operating conditions of a tidal turbine or any marine vehicle are simulated by towing the model by a carriage that moves back and forth at speeds ranging from 0.5 to 10 m/s. The carriage is powered by four Ward-Leonard electrical motors, providing precise control of velocity with an accuracy of 1 mm/s at constant speed. Additionally, the carriage allows for variable speed motion with user-defined acceleration laws. To generate waves, a single-paddle wave maker is located at the south end of the tank, while an absorbing beach is positioned at the opposite end to minimize wave reflections that could distort the wave patterns generated by the wave maker.

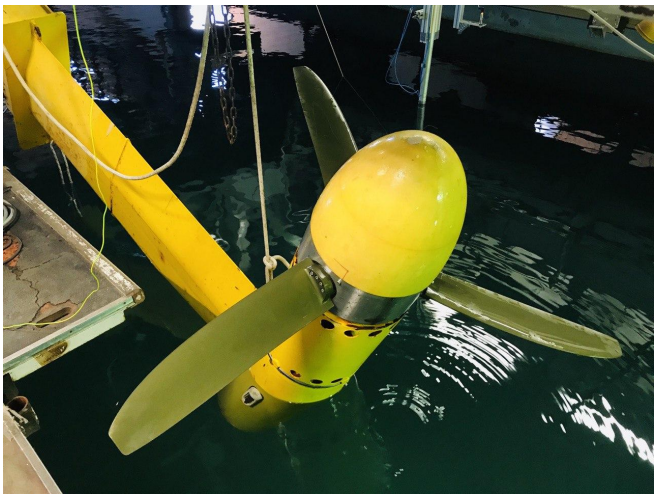

Fig. 3. The TTT model turbine with Schottel Hydro blades installed on the towing carriage at CNR-INM

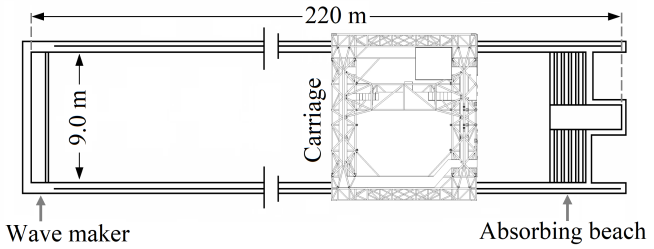

Fig. 4. Layout and dimensions of the wave-towing tank at CNR-INM

B. Instrumentation

The TTT model turbine was mounted on a support frame suspended from the towing carriage structure. The center of the turbine hub was positioned at a depth of 1.25 m below the still water surface, clamped from above by a steel stanchion in the mid-section of the tank.

In order to fully characterise the flow conditions, direct measurements were taken using two ultrasonic sensors to determine the wave pattern and a pitot velocimeter to measure the axial flow velocity intensity. These measurements allowed for the assessment of fluctuations in the current velocities caused by the waves and provided information on the kinematics of the waves. The pitot probe was positioned at a water depth corresponding to the blade tip when at the 12 o'clock position.

Top Fig. 5 depicts the carriage set-up with the TTT model turbine and part of the sensors, whereas bottom Fig. 5 shows a sketch of the set-up, with distances among turbine and sensors given in Table I.

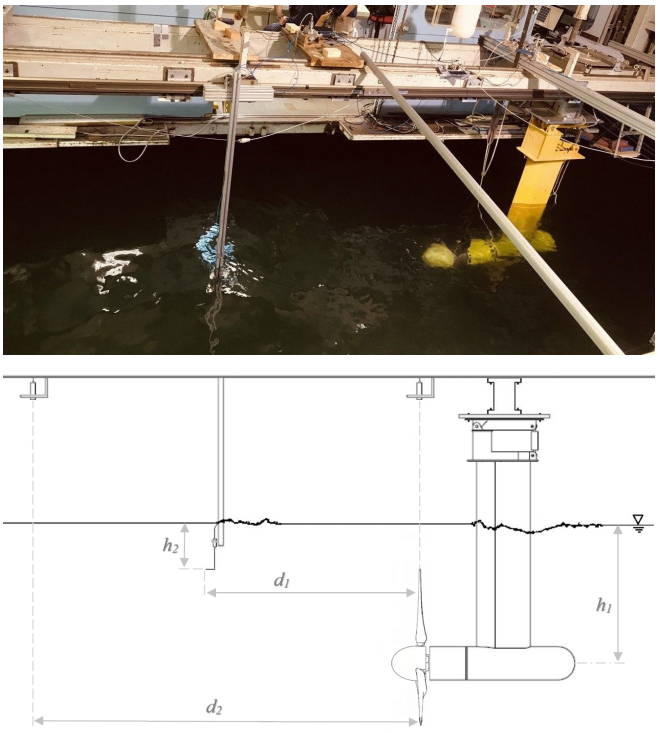

Fig. 5. TTT Turbine, flow velocity measurement (Pitot) and ultrasonic sensors deployment configuration.

TABLE I
TURBINE AND SENSORS DEPLOYMENT PARAMETERS

Symbol	Definition	Value [m]
h_1	Turbine depth	1.25
h_2	Pitot depth	0.50
d_1	Pitot distance from turbine blades	3.00
d_2	Ultrasonic distance from turbine blades	5.00

The velocimetry equipment consists of a Pitot tube with an ellipsoidal head of type L and a differential pressure measurement cell. The measurement cell has a range of ±1 to ±5000 PSI difference (PSID) with an output signal of $2mV/V$. The Pitot sensor enables the measurement of a single velocity component, with the axial component being measured during the tests. The Pitot tube has an intake at the nose for capturing the total pressure and 6 holes on the head for measuring the static pressure. Particular attention was paid to install the device in a vertical position, with the head, ending with an ellipsoidal nose, maintained parallel to the flow and facing it.

The measurement of the dynamic pressure P_d, which corresponds to the difference between the total pressure P_t captured by the nose and the static pressure P_s captured by the holes on the head, allows for the calculation of fluid velocity using the Bernoulli equation. The dynamic pressure is displayed by the instrument as "velocity pressure" in units of mmH_2O or Pa.

To quantitatively characterize the kinematics of waves in the tank, two metallic cylindrical ultrasonic sensors of size M18x1 were employed. The detection beam of each ultrasonic sensor has a conical shape with a base diameter of 400 mm and a penetration depth of 1500 mm. In the experimental set-up, the distance among sensors was carefully chosen to avoid interference causing noise in water level height acquisitions.

TABLE II
TEST MATRIX

Condition	Control strategy	Set-point
Calm water	Constant RPM	-
Regular wave I	SL-MPPT	7e-4
Regular wave I	TSR	5 & 6
Regular wave II	SL-MPPT	7e-4
Regular wave II	TSR	5 & 6

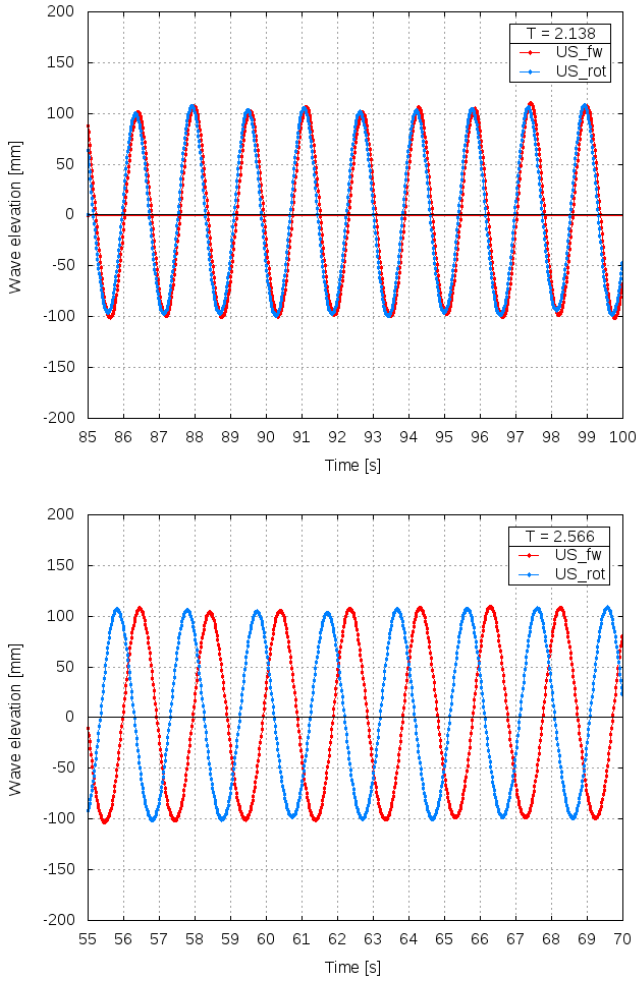

Fig. 6. Ultrasonic sensors – wavelength and wave elevation pattern

C. Experimental Scenarios

The tests were conducted in two scenarios: calm water (steady state) and unsteady inflow with regular (sinusoidal or monochromatic) waves, with two amplitude values chosen to simulate moderate sea-state conditions at full scale, and time scales comparable to turbine revolution periods. In addition to the proposed SL-MPPT control, a conventional TSR control method was also considered for comparative analysis.

The experimental scenarios are summarized in Table II, which includes the conditions, control strategies,

and set-points for each case. Based on previous experimental characterizations of the TTT model turbine [13], a reference value of the maximum (mechanical) power coefficient C_P = 0.44 at TSR = 5 was determined as the optimal condition. Based on these hydrodynamic characteristics and the PTO system characteristics of the TTT turbine, the theoretical value of K_{dc} obtained from (9) is approximately K_{dc} = 7e-4, which is taken as set-point for SL-MPPT control.

Initially, a series of experiments with constant RPM were conducted in calm water to establish the baseline performance characteristics of the turbine. A constant flow speed between 0.8 and 1.4 m/s was considered. These experiments were instrumental in tracking and assessing the effect of alternative control strategies, such as TSR and SL-MPPT, on turbine operation under unsteady flow conditions.

Next, two regular waves in-line with the current were generated in the tank to establish onset flow conditions characterized by a fluctuating components superimposed on the carriage speed, which was maintained constant at $V_F = 1.2$ m/s. Specifically, the wave paddle in the tank was set to generate regular patterns with 200 mm nominal wave height H_w, and encountering frequency T_w of 2.138 and 2.566 seconds. At TSR=5 and $V_F = 1.2$ m/s, the wave periods correspond, respectively, to 2 and 2.5 turbine revolution periods. The generated free-surface flow is described by a Froude number $Fn = 0.31$, calculated as $Fn = V_F/\sqrt{gD}$, with $g = 9.806$ ms^{-2}.

Fig. 6 shows wavelength and wave elevation pattern as measured by the ultrasonic sensors for the two wave cases and a representative time period of 15 seconds. The waves come across the turbine with a regular pattern and the wave elevation fairly matches the imposed value. The phase shift between the two signals is a consequence of the position of the two probes, as illustrated in Fig. 5. In particular, in the testing conditions at T_w of 2.138 s, the signals measured by the two probes are almost in phase.

In both calm-water and wave conditions, the proposed SL-MPPT control strategy was compared with two TSR control references: TSR = 5 (design point) and TSR = 6 (over-speed zone).

IV. Results and Analysis

This section presents the results obtained from the experiments described in Section III. Measured data were analyzed to assess the effectiveness of the SL-MPPT strategy in optimizing power extraction from the TTT model turbine.

As mentioned above, the results obtained using the constant RPM strategy in calm water operation were considered as a reference to identify turbine performance figures. This choice is motivated by the fact that under calm water towing and with constant RPM control, the turbine operating conditions are precisely known (onset flow speed and optimum rotation speed) without the need for input from flow measurement sensors. Subsequently, the optimal value for the K_{dc} coefficient in Eq. (9), which mediates the relationship between the DC-bus current and the square of the DC-bus voltage, was established for the case with an inflow speed of 1.2 m/s. The mean value obtained from the calm water test was $K_{dc} = 6.8\,\mathrm{e}^{-4}$, in very good agreement with the theoretical value taken as the set-point for the SL-MPPT control.

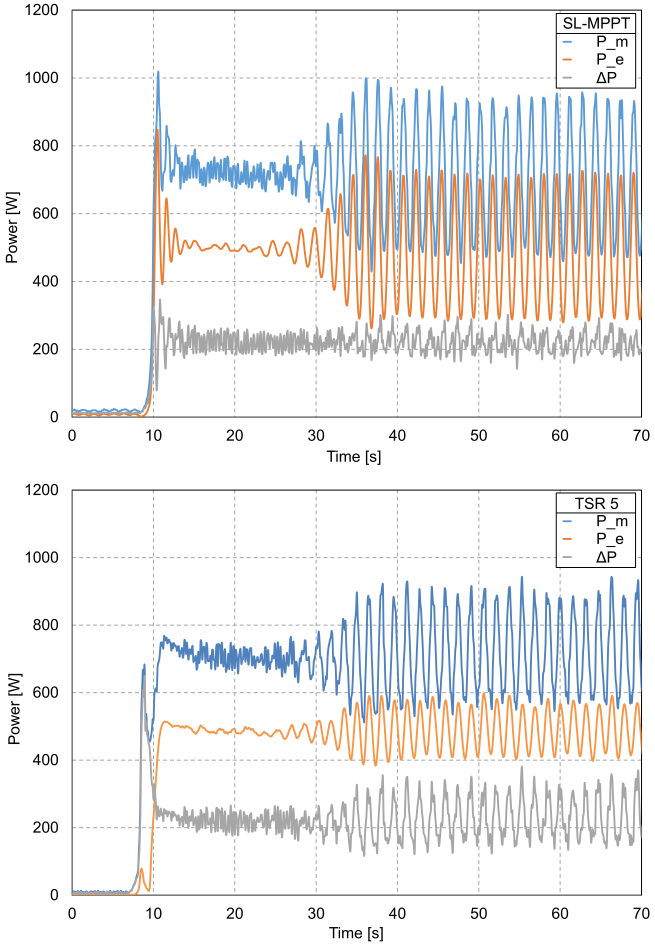

Fig. 7. Time series of generated mechanical power P_m, electrical power P_{el}, and dissipated power ΔP with the SL-MPPT control (top), and TSR (bottom). Wave–towing conditions at $T_w = 2.138$ s.

Figure 7 shows the time series of mechanical power P_m, electrical power P_{el}, under the SL-MPPT and TSR control strategies facing inflow fluctuations caused by surface waves with period $T_w = 2.138$ s. This figure describes how wave–towing tests are performed. At time $t = 0$, the wave generator is activated and at the opposite side of the tank the carriage starts moving. After few seconds, the generated wave train encounters the towed turbine. In the cases described in Fig. 7, this condition happens at approximately time $t_e = 30$ s. After about 10 seconds, fully developed regular waves interact with the turbine. Both power signals oscillate with the wave–forcing frequency. The intensity of fluctuations with SL-MPPT control (top Fig. 7) is higher than in the TSR control case (bottom Fig. 7). Another difference is that while in the SL-MPPT control case, the fluctuations of mechanical and electrical power have a comparable intensity, in the TSR control case, the electrical power oscillates with significantly lower intensity than the mechanical power. This is reflected by the difference between mechanical and electrical

power, $\Delta P = P_m - P_{el}$, with strong oscillations in the TSR control case.

The quantity ΔP denotes the passive power dissipated by the PTO components, encompassing the generator, the power electronic interface, and the drive-train (shaft, joints, and gearbox). In fact, it represents the portion of mechanical power that is dissipated into heat and fatigue loads on the turbine mechanical parts. The results displayed in Fig. 7 reveal that the passive power, under both control strategies, remains relatively stable prior to the onset of inflow fluctuations, indicating the PTO system's efficiency, which is independent of the control strategy employed. However, during unsteady flow conditions (from approximately $t_e = 30$ s), this characteristic persists only in the case of SL-MPPT control, whereas intense peaks of passive power occur when using TSR control. The same trend was observed with wave forcing at $T_w = 2.566$ s (not shown). This phenomenon suggests that the SL-MPPT control strategy effectively tracks the dynamics of the onset flow and compensates for the variability of conditions to maintain peak power point operation.

To gain a better understanding of the effect of alternative control strategies on turbine operation, a comparison is made between the fluctuation of turbine power performances and the corresponding quantities measured when the turbine operates in a constant and uniform onset flow without waves (calm water).

Figure 8 shows instant measurements of mechanical power in wave–towing conditions at $T_w = 2.138$ s (top) and $T_w = 2.566$ s (bottom), and using different control strategies and set-points. Unsteady flow measurements are compared with calm water test data with constant RPM control at flow speed 0.8, 1.1, 1.2, and 1.4 m/s, and their polynomial fit. Both results under SL-MPPT and TSR control describe loops that correspond to several wave periods with quasi identical conditions as shown in Fig. 6.

Mechanical power mean values, plotted as colored square dots, are approximately matching the calm water condition at $V_F = 1.2$ m/s. A major difference between control strategies is that SL-MPPT data describe loops where at each time step the measured power is close to the calm water value at the same instant velocity. A completely different trend is observed by using the TSR control, with very large oscillations of measured power.

Similar comparisons are presented for the turbine power coefficient C_P and torque coefficient C_Q versus TSR, in Figs. 9 and 10, respectively. In this case, the turbine power coefficient C_P, the tip speed ratio λ and the torque coefficient $C_Q = C_P/\lambda$ have been evaluated by modified definitions in (1) and (2), where the nominal flow speed V_F is replaced with the actual value of the axial velocity incoming to the turbine under the effect of surface waves. As a reference, instant values of power and torque coefficients in the wave–towing case are compared with results of calm water tests described in [21], where a 0.5 m diameter model turbine with same blade design as the TTT turbine was tested in a flume tank at flow speed up to 2.75 m/s.

The results clearly show the effect of the control

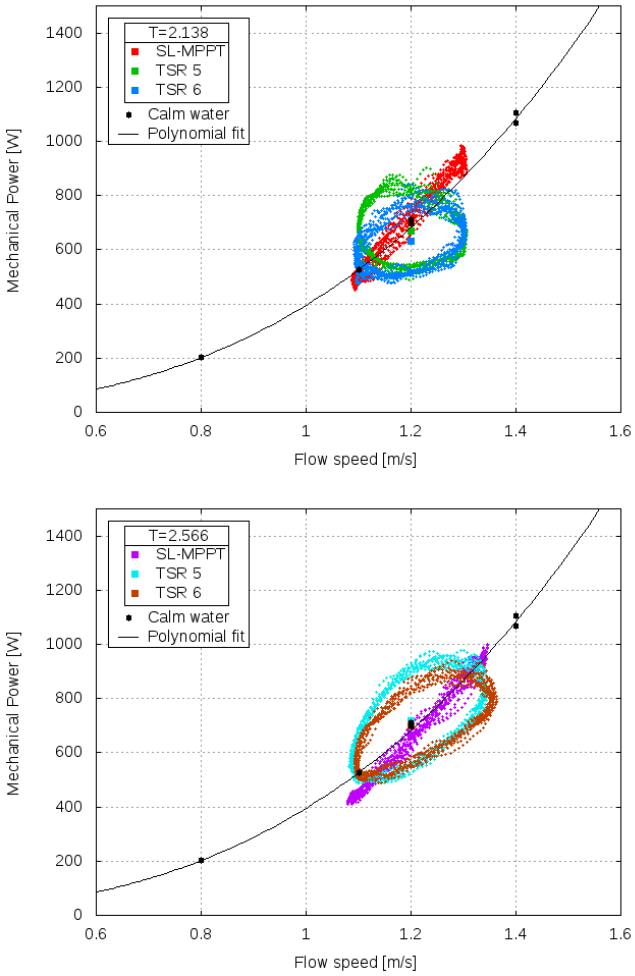

Fig. 8. Mechanical power versus actual flow speed with SL-MPPT and TSR 5, 6 controls. Wave–towing conditions at $T_w = 2.138$ s (top) and $T_w = 2.566$ s (bottom), and comparison with calm water measurements.

strategy on the variability of the mechanical torque and power output of the turbine when subjected to a variable onset flow. These comparisons provide valuable insights into the response of the control strategies, with reference to the capability to track the optimal operating condition, and to limit the intensity of load fluctuations on turbine blades and drive-train components.

In particular, it can be observed that the proposed SL-MPPT control strategy determines smaller fluctuations in mechanical power compared to the TSR control strategy. The SL-MPPT results closely match the turbine response during ideal uniform flow conditions. In contrast, the TSR–based control leads to relatively strong oscillations in mechanical loads compared to uniform flow operation at the same speed. This common feature can be attributed to the uncertainty in evaluating the onset flow speed required by the control strategy and the limitations in the dynamic response of the physical control.

The obtained results highlight that the turbine rotational speed adapts to unsteady inflow conditions through the quick dynamic response of the SL-MPPT control strategy. As a result, in spite of the wave–induced velocity fluctuations, turbine operation at the

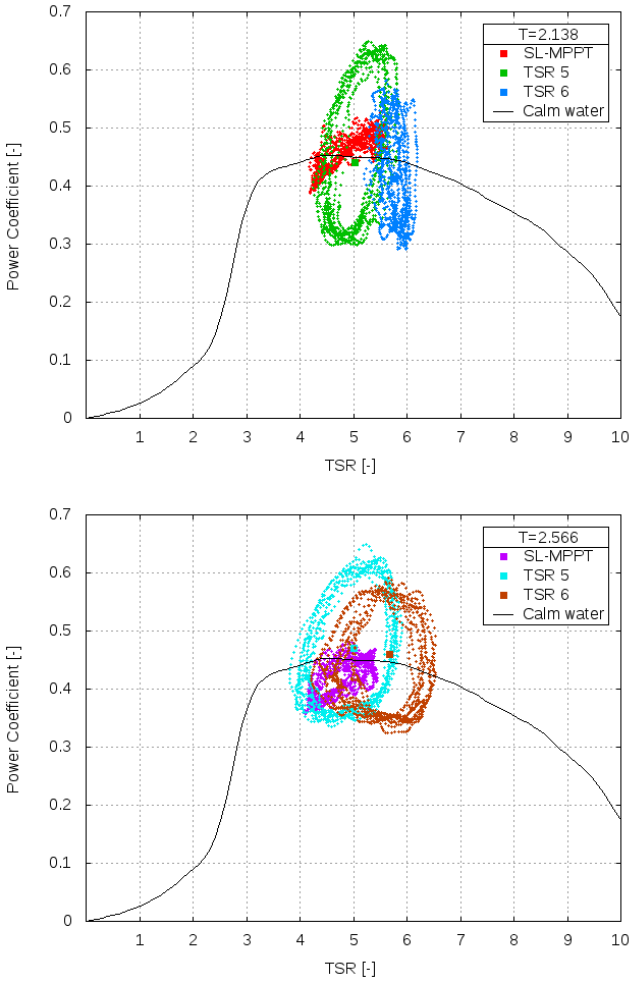

Fig. 9. Instant values of power coefficient C_P versus instant TSR. Wave–towing conditions at $T_w = 2.138$ s (top) and $T_w = 2.566$ s (bottom), and comparison with calm water data from [21].

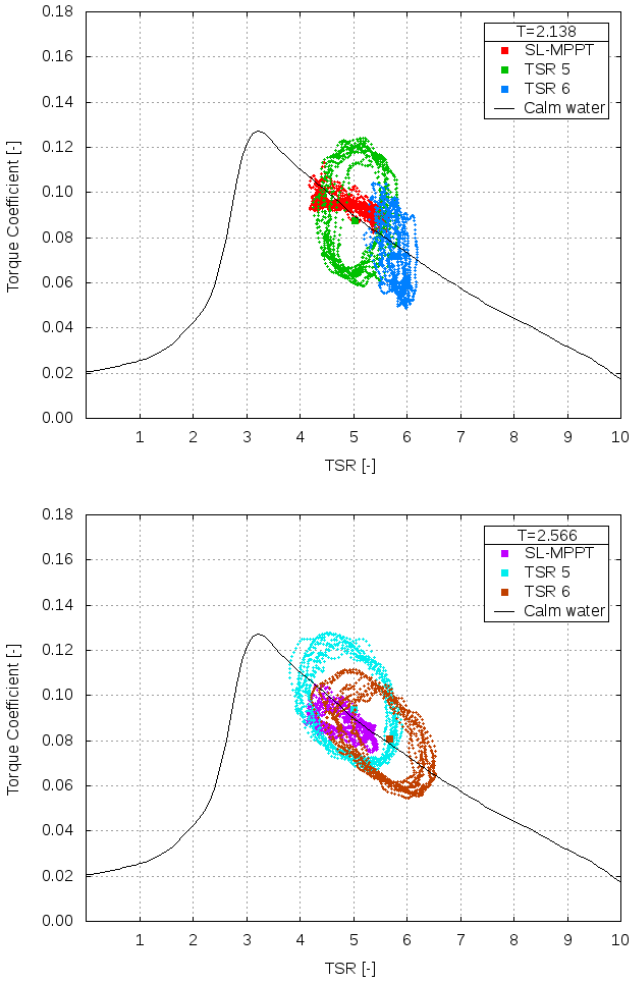

Fig. 10. Instant values of power coefficient C_Q versus instant TSR. Wave–towing conditions at $T_w = 2.138$ s (top) and $T_w = 2.566$ s (bottom), and comparison with calm water data from [21].

maximum power coefficient is enforced, thus optimizing power extraction in transient inflow conditions.

V. Conclusion

The effectiveness of a novel mechanical Sensor-Less Maximum Power Point Tracking (SL-MPPT) control for tidal stream turbines under fluctuations of the onset flow has been investigated. The control methodology has been outlined, and the results of validation studies by towing tank experiments have been discussed.

A key aspect of the proposed control strategy is that the turbine power take-off response is governed by maintaining a constant ratio between the generator current and the square of the DC-bus voltage. The optimal proportionality factor can be determined from turbine performance in uniform flow conditions at constant RPM.

The study was conducted at the wave–towing tank facility at CNR-INM, using a 3–bladed, horizontal-axis model turbine with a 1.5 m diameter, developed at the Queen's University of Belfast. The turbine was equipped with Schottel Hydro blades, a Permanent Magnet Synchronous Generator (PMSG) with a single-stage gearbox, and a central data acquisition system suitable for implementing alternative control strategies.

Preliminary tests in calm water conditions determined a proportionality factor in close agreement with the theoretical value predicted by the simulation model used to develop the methodology. The capability of the proposed SL-MPPT control strategy to track the optimal turbine operating point in variable inflow conditions was investigated by towing tests in regular waves with periods equal to 2 and 2.5 turbine revolution periods and Froude number $Fn = 0.31$. The analysis of the response of the turbine with SL-MPPT control and a conventional TSR control allows to draw some conclusions:

- under the SL-MPPT control, the electrical power follows the fluctuations of the mechanical power associated to the onset flow perturbation;
- the power that is dissipated in the mechanical/electrical conversion presents very small oscillations with respect to the variability of the rotor loadings;
- regardless of the wave–induced variability of the inflow speed, the mechanical power delivered with the SL-MPPT control presents fluctuations around optimal calm water conditions at the same instant flow speed that are very small as compared to TSR control operation;

- a similar trend is observed for the mechanical torque.

The analysis of turbine performance covering a wide range of loading conditions and inflow variability is the subject of ongoing work. The objective is to confirm the promising results obtained from the present laboratory tests and from available field site data and assess the proposed methodology as an alternative to conventional control strategies used in the tidal energy sector.

ACKNOWLEDGEMENT

The authors wish to thank Dr. Ralf Starzmann at Schottel Hydro, Mr. Cuan Boake at Applied Renewables Research Ltd. for their contributions, and the CNR-INM staff who supported testing activities. Part of the work was funded under the H2020 MaRINET-2 TNA Project 'TTT-maxP.'

REFERENCES

[1] IRENA and OEE, "Scaling up investments in ocean energy technologies," Abu Dhabi. ISBN 978-92-9260-528-5, 2023.

[2] L. Myers and A. S. Bahaj, "Simulated electrical power potential harnessed by marine current turbine arrays in the alderney race," *Renewable energy*, vol. 30, no. 11, pp. 1713–1731, 2005.

[3] M. Thiébaut, J.-F. Filipot, C. Maisondieu, G. Damblans, R. Duarte, E. Droniou, N. Chaplain, and S. Guillou, "A comprehensive assessment of turbulence at a tidal-stream energy site influenced by wind-generated ocean waves," *Energy*, vol. 191, p. 116550, 2020. [Online]. Available: https://www.sciencedirect.com/science/article/pii/S0360544219322455

[4] I. Milne, A. Day, R. Sharma, and R. Flay, "The characterisation of the hydrodynamic loads on tidal turbines due to turbulence," *Renewable and Sustainable Energy Reviews*, vol. 56, pp. 851–864, 2016. [Online]. Available: https://www.sciencedirect.com/science/article/pii/S1364032115013623

[5] T. de Jesus Henriques, S. Tedds, A. Botsari, G. Najafian, T. Hedges, C. Sutcliffe, I. Owen, and R. Poole, "The effects of wave–current interaction on the performance of a model horizontal axis tidal turbine," *International Journal of Marine Energy*, vol. 8, pp. 17–35, 2014.

[6] S. Tatum, C. Frost, M. Allmark, D. O'doherty, A. Mason-Jones, P. Prickett, R. Grosvenor, C. Byrne, and T. O'Doherty, "Wave–current interaction effects on tidal stream turbine performance and loading characteristics," *International Journal of Marine Energy*, vol. 14, pp. 161–179, 2016.

[7] S. Ordonez Sanchez, K. Porter, C. Frost, M. Allmark, C. Johnstone, and T. O'Doherty, "Effects of extreme wave-current interactions on the performance of tidal stream turbines," in *3rd Asian Wave and Tidal Energy Conference*, 2016.

[8] R. Martinez, G. S. Payne, and T. Bruce, "The effects of oblique waves and currents on the loadings and performance of tidal turbines," *Ocean Engineering*, vol. 164, pp. 55–64, 2018.

[9] B. Gaurier *et al.*, "Marinet2 tidal energy round robin tests-performance comparison of a horizontal axis turbine subjected to combined wave and current conditions," *Journal of Marine Science and Engineering*, vol. 8, no. 6, p. 463, 2020.

[10] M. J. Beam, B. L. Kline, B. E. Elbing, W. Straka, A. A. Fontaine, M. Lawson, Y. Li, R. Thresher, and M. Previsic, "Marine hydrokinetic turbine power-take-off design for optimal performance and low impact on cost-of-energy," in *International Conference on Offshore Mechanics and Arctic Engineering*, vol. 55423. American Society of Mechanical Engineers, 2013, p. V008T09A041.

[11] J. G. Njiri and D. Söffker, "State-of-the-art in wind turbine control: Trends and challenges," *Renewable and Sustainable Energy Reviews*, vol. 60, pp. 377–393, 2016.

[12] A. R. Nejad *et al.*, "Wind turbine drivetrains: state-of-the-art technologies and future development trends," *Wind Energy Science*, vol. 7, no. 1, pp. 387–411, 2022.

[13] M. Rafiei, F. Salvatore, C. Frost, and I. Benson, "Field tests validation of a mechanical sensor-less mppt control strategy for tidal turbines." in *The 33rd International Ocean and Polar Engineering Conference*, 2023.

[14] C. Frost, I. Benson, B. Elsäßer, R. Starzmann, and T. Whittaker, "Mitigating uncertainty in tidal turbine performance characteristics from experimental testing," in *Proceedings of the European Wave & Tidal Energy Conference, Cork, Ireland*, vol. 27, 2017.

[15] M. Rafiei, F. Salvatore, and F. Giulii Capponi, "Generator topologies for horizontal axis tidal turbine," in *ELECTRIMACS 2019: Selected Papers-Volume 1*. Springer, 2020, pp. 447–459.

[16] R. J. Cavagnaro, B. Polagye, J. Thomson, B. Fabien, D. Forbush, L. Kilcher, J. Donegan, and J. McEntee, "Emulation of a hydrokinetic turbine to assess control and grid integration," in *Proceedings of the 11th European Wave and Tidal Energy Conference, Nantes, France*, 2015.

[17] M. Moreau, G. Germain, G. Maurice, and A. Richard, "Sea states influence on the behaviour of a bottom mounted full-scale twin vertical axis tidal turbine," *Ocean Engineering*, vol. 265, p. 112582, 2022.

[18] P. Jeffcoate, F. Salvatore, C. Boake, and B. Elsaesser, "Effect of submergence on tidal turbine performance," in *Proceedings of the 11th European Wave and Tidal Energy Conference, Nantes, France*, 2015.

[19] N. Mohan, T. M. Undeland, and W. P. Robbins, *Power electronics: converters, applications, and design*. John wiley & sons, 2003.

[20] N. Kaufmann, T. Carolus, and R. Starzmann, "Turbines for modular tidal current energy converters," *Renewable Energy*, vol. 142, pp. 451–460, 2019.

[21] Z. Sarichloo, F. Salvatore, F. Di Felice, M. Costanzo, R. Starzmann, and C. Frost, "Computational analysis and experimental verification of a boundary integral equation model for tidal turbines," in *Advances in Renewable Energies Offshore: Proceedings of the 3rd International Conference on Renewable Energies Offshore (RENEW 2018), October 8-10, 2018, Lisbon, Portugal*. CRC Press, 2018, p. 209.